Physics of the Earth and Planetary Interiors 172 (2009) 235–240

Contents lists available at ScienceDirect

Physics of the Earth and Planetary Interiors

journal homepage: www.elsevier.com/locate/pepi

Elasticity of stishovite and acoustic mode softening under high pressure by Brillouin scattering

Fuming Jiang[a,*], Gabriel D. Gwanmesia[b], Tatiyana I. Dyuzheva[c], Thomas S. Duffy[a]

[a] Department of Geosciences, Princeton University, Princeton, NJ 08544, United States
[b] Department of Physics and Pre-Engineering, Delaware State University, Dover, DE 19901, United States
[c] Institute of High-Pressure Physics, Troitsk, 142190 Moscow, Russia

ARTICLE INFO

Article history:
Received 29 February 2008
Received in revised form
10 September 2008
Accepted 23 September 2008

Keywords:
Elasticity
Stishovite
High-pressure
Silica

ABSTRACT

Brillouin scattering measurements on single-crystal stishovite, a high-pressure polymorph of SiO_2, were carried out to 22 GPa. Acoustic velocities in three 30-μm thick crystal platelets of synthetic stishovite were measured in a forward symmetric scattering geometry, and the full set of elastic constants were retrieved to 12 GPa. The measured velocity data were fit to Christoffel's equation, yielding ambient-pressure elastic constants of C_{11} = 455(1) GPa, C_{33} = 762(2) GPa, C_{12} = 199(2) GPa, C_{13} = 192(2) GPa, C_{44} = 258(1) GPa, and C_{66} = 321(1) GPa. The elastic modulus $(C_{11} - C_{12})/2$ was observed to decrease with pressure, indicating acoustic mode softening, consistent with theoretical predications for the behavior of stishovite as it approaches the transition to the $CaCl_2$-type phase. The bounds on the aggregate adiabatic bulk and shear moduli are K_{S0} = 315(1) GPa, G_0 = 240(1) GPa for the Voigt bound, K_{S0} = 301(1) GPa, G_0 = 216(1) GPa for the Reuss bound. Pressure derivatives of aggregate bulk and shear moduli were constrained to be $(\partial K_S/\partial P)_{T0}$ = 4.34(16) and $(\partial G/\partial P)_0$ = 0.7(1) for the Reuss bound, and $(\partial K_S/\partial P)_{T0}$ = 4.0(1) and $(\partial G/\partial P)_0$ = 1.1(1) for the Voigt–Reuss–Hill (VRH) average, respectively, by fitting the data to Eulerian finite strain equations. The volume compression curve obtained from our Brillouin measurement is in very good agreement with previous compression studies up to 50 GPa.

1. Introduction

Stishovite, a six-coordinated polymorph of silica, SiO_2, is of great interest for the mineralogy of the Earth's mantle and for understanding the fundamental physics of phase transformations (Hemley et al., 1994). In the Earth's interior, stishovite is expected to be an important constituent in basaltic compositions (Irifune and Ringwood, 1993; Kesson et al., 1994; Hirose and Fei, 2002) and deeply subducted sediments (Irifune et al., 1994; Dobrzhinetskaya and Green, 2007).

Theoretical and experimental studies reveal that stishovite transforms to an orthorhombic $CaCl_2$-type structure around 50 GPa (Cohen, 1992; Kingma et al., 1995). This transition may contribute to unexplained seismic structure in the Earth's lower mantle (Karki et al., 2001; Vinnik et al., 2001; Lakshtanov et al., 2007a,b). According to theoretical models, the phase transition is trigged by the lattice instability of a soft transverse acoustic mode associated with the shear elastic constant $(C_{11} - C_{12})/2$ (Cohen, 1992). Many AX_2 compounds with the rutile structure undergo a transition to $CaCl_2$-type phase under pressure (e.g., Hellwig et al., 2003). Therefore, it is of interest to measure the elastic constant tensor of stishovite under high pressure to improve understanding of this phase transition (Carpenter et al., 2000) and its potential effect on seismic structure in the Earth's mantle.

The elastic constants of stishovite were measured previously at ambient conditions by Brillouin spectroscopy (Weidner et al., 1982; Brazhkin et al., 2002, 2005). The bulk modulus, K_{T0}, and its pressure derivative, $K'_{T0} = (\partial K_T/\partial P)_{T0}$, as obtained by compression studies (Ross et al., 1990; Andrault et al., 1998, 2003; Liu et al., 1999; Hemley et al., 2000; Yamanaka et al., 2002; Luo et al., 2002; Panero et al., 2003; Nishihara et al., 2005) exhibit a wide range of values, in particular for the value of K'_{T0}. Li et al. (1996) performed ultrasonic measurements on polycrystalline samples to 3 GPa, and gave the first reported pressure derivatives of the adiabatic bulk and shear modulus ($K'_{T0} = 5.3 \pm 0.1$, $G'_0 = 1.8 \pm 0.1$). The discrepancies among previous experiments indicate a need for precision measurement on single-crystal samples at high pressure using the Brillouin spectroscopy technique.

Stishovite can incorporate both hydrogen and aluminum as a coupled substitution. In Al-free samples, the maximum H content is found to be only 45 ± 29 H per 10^6 Si atoms (Pawley et al., 1993) or less (Bromiley et al., 2006). The effect of simultaneous H and

* Corresponding author. Tel.: +1 609 258 3261.
E-mail address: fumingj@princeton.edu (F. Jiang).

0031-9201/$ – see front matter © 2008 Elsevier B.V. All rights reserved.
doi:10.1016/j.pepi.2008.09.017

Al incorporation has been studied by both theory and experiments (Ono et al., 2002; Panero and Stixrude, 2004; Litasov et al., 2007). The equation of state of Al_2O_3- and H_2O-bearing stishovite has been examined by Ono et al. (2002) and Lakshtanov et al. (2005) showing reduction of the bulk modulus relative to SiO_2 stishovite. Lakshtanov et al. (2007a) reported a linear decrease of the acoustic velocities and elastic moduli as a function of Al^{3+} concentration, and they concluded that the formation of oxygen vacancies has a stronger effect on the density and elastic properties of stishovite than does the incorporation of hydrogen. The incorporation of Al can also significantly lower the rutile to $CaCl_2$-type phase transition pressure (Lakshtanov et al., 2007b).

In this study, we report acoustic velocity measurements in each of three crystal planes of stishovite over 18 crystallographic directions up to 12 GPa and on one of them up to 22 GPa. Individual elastic constants were retrieved by fitting the measured velocities to the Christoffel's equation, and the aggregate bulk and shear moduli were then derived from the C_{ij}s. Pressure derivatives are obtained by fitting to finite strain equations. The results are compared with previous experimental and theoretical studies.

2. Experiments

Stishovite single crystals used in this study were grown in a 1500-ton Kawai-type multi-anvil apparatus at the Geophysical Laboratory of the Carnegie Institution of Washington. The crystals were grown in a 14/8 cell assembly (Gwanmesia and Liebermann, 1992) utilizing $LaCrO_3$ as a resistance heater. High-grade amorphous silica powder was ground in alcohol and loaded in a platinum capsule. The capsule was pressure-sealed and placed in a MgO sleeve within the cylindrical $LaCrO_3$ furnace. The synthesis experiment was conducted at 12 GPa and 1500 °C for 4 h, resulting in several crystals ranging in dimensions from 10 to 1000 μm throughout the capsule.

The crystals were characterized by synchrotron X-ray diffraction at X17C of National Synchrotron Light Source, Brookhaven National Laboratory and the lattice parameters were determined to be: $a = 4.1746(8)$ Å, $c = 2.6625(3)$ Å. Raman spectroscopy was also used to characterize our samples, and the four characteristic Raman peak positions of stishovite are in excellent agreement ($\pm 1\ cm^{-1}$) with those of natural and synthetic stishovite (Hemley et al., 1986), and an extremely weak OH-band was observed, indicating a very low H concentration.

More than six as-grown stishovite single crystals were double side polished to a final thickness of about 30 μm using successively finer diamond abrasive films down to a grit size of 1 μm. High-pressure Brillouin measurement of stishovite in the diamond anvil cell is challenging because of the overlapping of stishovite P-wave with the diamond S-wave. To circumvent this problem, the velocity curves of two diamond anvils were first measured, and two anvils were then aligned in the same crystallographic orientation. Secondly, six randomly polished crystal platelets of stishovite were measured at ambient conditions to determine their velocity curves. By comparing the measured stishovite P-wave and diamond S-wave velocity curves, three crystals were chosen for high-pressure Brillouin measurement based on the criteria that the stishovite P-wave and diamond S-wave can be separated in at least some specific directions by orienting the crystal relative to the two diamonds. The chosen crystals were then loaded in modified Merrill–Basset diamond cells with angular opening of 96° and positioned appropriately with respect to the anvils. Stainless steel gaskets were pre-indented to about 50-μm thickness and a 250-μm hole was drilled in the center. A 16:3:1 methanol–ethanol–water mixture was used as pressure transmitting medium, and rubies were placed around the crystal in the diamond cell as a pressure standard.

A single-frequency vertically polarized solid state Nd:vanadate laser with a wavelength of 532.15 nm and a power of 150 mW was used. The Brillouin spectra were collected in a forward symmetric scattering geometry with an external angle of 70° and analyzed using a six-pass Sandercock tandem Fabry–Perot interferometer. Acoustic velocities were measured in three crystal platelets at ambient and 9 elevated pressures to 12 GPa, and one of the three crystal platelets was measured to 22 GPa. Above 12 GPa, the diamond cell was annealed to alleviate deviatoric stress; pressure differences determined from different rubies were about ±0.5 GPa for pressures below 15 GPa and about ±1 GPa for pressures above 15 GPa. At each pressure, Brillouin spectra were collected in more than 37 directions over an angular range of 180° with a 5° step. Further experimental details can be found elsewhere (Speziale and Duffy, 2002; Jiang et al., 2004; Speziale et al., 2004).

3. Results and discussion

Fig. 1 shows a typical Brillouin spectrum collected at 9.4 GPa. For this particular direction, one stishovite P-wave and one S-wave were observed in addition to the peaks from the pressure medium and diamond. Because the two diamond anvils were aligned, they appear as a single diamond S-wave peak.

Stishovite crystallizes in the tetragonal system (space group: $P4_2/mnm$) with six independent non-zero elastic constants: C_{11}, C_{12}, C_{13}, C_{33}, C_{44}, and C_{66}. For each crystal platelet, three Eulerian angles are used to specify its crystal orientation. At each pressure, the measured velocity data in three crystal platelets were fit together to Christoffel's equation:

$$|C_{iklm}q_kq_l - \rho V^2\delta_{im}| = 0$$

where ρ is the density, V is the acoustic velocity, q_i is the acoustic wave vector, C_{iklm} is the elastic constant in full suffix notation. Nonlinear least squares inversion was used to obtain individual elastic constants and the three Eulerian angles from the measured velocity data (Speziale and Duffy, 2002; Jiang et al., 2004). The root-mean-square (RMS) differences between the measured and calculated acoustic velocities are around $56\ m\ s^{-1}$ at ambient condition and $90\ m\ s^{-1}$ at high pressures. Fig. 2 compares measured and best-fit velocity data for the three crystal platelets at ambient conditions and a pressure of 8 GPa.

Using the retrieved elastic constants, the Reuss and Voigt bounds, and Voigt–Reuss–Hill (VRH) average of the adiabatic

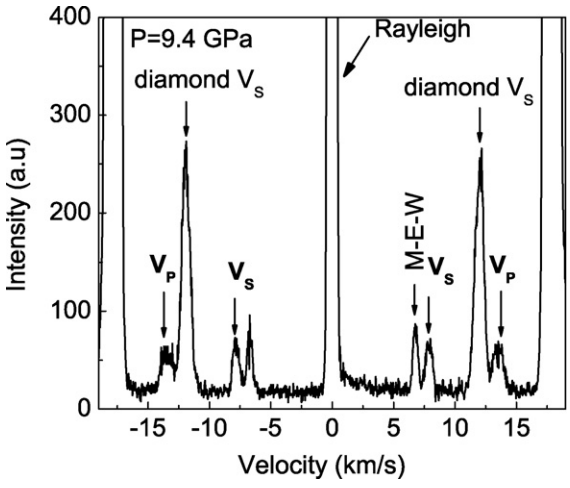

Fig. 1. Example Brillouin spectrum collected at 9.4 GPa. M–E–W: methanol–ethanol–water pressure medium.

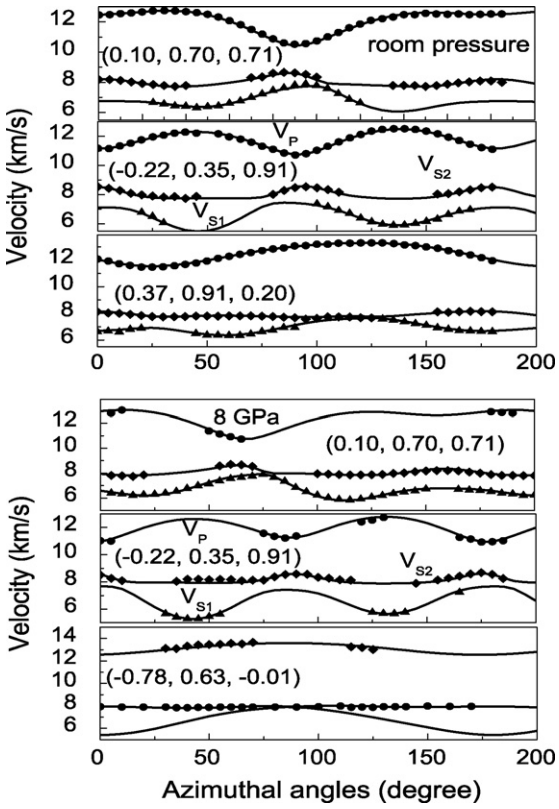

Fig. 2. Velocities in stishovite at ambient conditions (upper panel) and at 8 GPa (lower panel): symbols show measured velocities and solid curves are obtained from best-fit elastic constants. Orientation of each plane is indicated. Different planes were used at ambient and high pressures for lower panel.

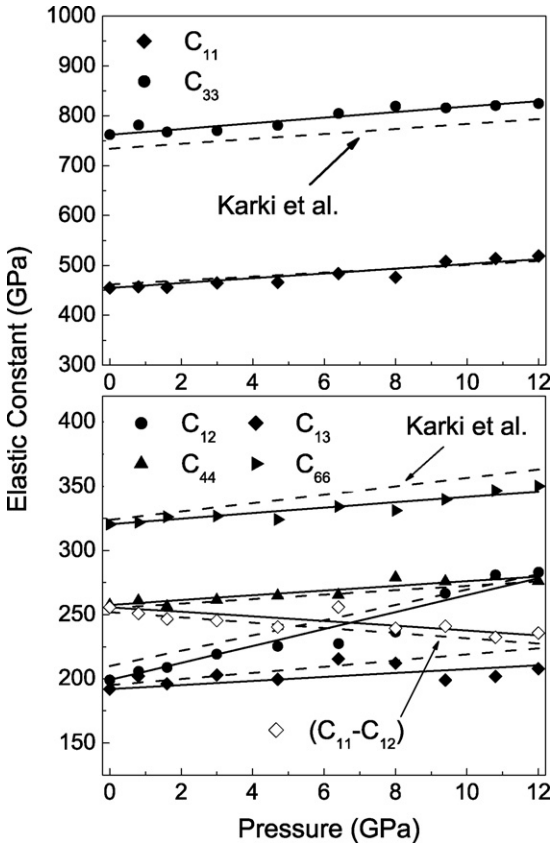

Fig. 3. Pressure dependences of elastic constants: symbols are from experiments; solid lines are best fits to finite strain equations; dashed lines are from theory (Karki et al., 1997).

aggregate bulk and shear moduli were calculated and fit to the third-order Eulerian finite strain equation (Birch, 1978) to obtain the adiabatic K_{S0} and $K'_{S0} = (\partial K_S/\partial P)_{T0}$. The isothermal aggregate bulk modulus, K_{T0}, and its derivative, K'_{T0}, were obtained by applying appropriate thermodynamic relations (Speziale and Duffy, 2002). The parameters used in the conversion are the volume thermal expansion $\alpha_0 = 1.26 \times 10^{-5}\,K^{-1}$, $(\partial K_T/\partial T)_P = -0.046\,GPa\,K^{-1}$ (Nishihara et al., 2005), and specific heat $C_P = 41.5\,J\,mol^{-1}\,K^{-1}$ (Akaogi et al., 1995). Fig. 3 shows individual elastic constants as a function of pressure: symbols are from the experiment and solid lines are best-fits to the Eulerian finite strain equations, dashed lines are from theoretical calculations (Karki et al., 1997). Table 1 lists the individual elastic moduli and pressure derivatives in comparison with previous theoretical and experimental studies (Weidner et al., 1982; Holm and Ahuja, 1999; Karki et al., 1997, 2001; Brazhkin et al., 2002, 2005); experimental values of pressure derivatives of individual elastic constants are reported here for the first time. Our ambient-pressure C_{ij}s are generally in reasonable agreement with those from previous experimental and theoretical studies. To confirm the reliability of the present measurement, a 90° Brillouin scattering was performed on a single crystal from another source (Brazhkin et al., 2002). The crystal has a prismatic habit with four perpendicular (1 1 0) faces (Bendeliani, 2002). The incident laser was focused along one (1 1 0) face and the scattered light was collected through an orthogonal face ($1\bar{1}0$). This results in a phonon propagation direction along [1 0 0]. In this particular scattering geometry, two elastic moduli were obtained: $C_{11} = 458$ GPa, and $C_{44} = 263$ GPa using refractive index: $n_o = 1.799$ and $n_e = 1.826$ (Brazhkin et al., 2005). They are consistent with our results in forward scattering geometry and those reported by Brazhkin et al. (2005). To further check the reliability of the present study, single crystal synchrotron X-ray diffraction at X17C of the National Synchrotron Light Source was used to determine the three crystal orientations at room pressure: (0.15, 0.73, 0.67), (−0.20, 0.30, 0.93) and (0.35, 0.92, 0.15). They are consistent within about 3° with the orientations of (0.10, 0.70, 0.71), (−0.22, 0.35, 0.91) and (0.37, 0.91, 0.20) determined by fitting our velocity data.

Stishovite exhibits strong elastic anisotropy. C_{33} is the largest among all individual constants and it is about 1.7 times the value of C_{11}. This is explained by the stishovite crystal structure in which six-coordinated Si octahedra are edge-shared along the *c*-axis and corner-shared along *a*-axis, resulting in strong bonding along *c*. Of all the individual elastic constants, it is interesting to note that C_{12} has a very large pressure derivative $C'_{12} = 6.6(4)$ in comparison with a pressure derivative of $C'_{13} = 1.6(3)$, and this value is

Table 1
Elastic moduli and their pressure derivatives for stishovite.

	Elastic moduli (in GPa)					
	C_{11}	C_{33}	C_{12}	C_{13}	C_{44}	C_{66}
This study	455(1)	762(1)	199(2)	192(1)	258(1)	321(1)
Weidner et al. (1982)	453(4)	776(5)	211(5)	203(4)	252(2)	302(3)
Brazhkin et al. (2005)	466(3)	775(4)	207(8)	204(4)	258(2)	310(6)
Brazhkin et al. (2002)	463	757	205	203	252	298
Karki et al. (1997)	462	734	210	195	255	324
Holm and Ahuja (1999)	480	735	245	220	260	340
	Pressure derivatives of C_{ij}					
	$\partial C_{11}/\partial P$	$\partial C_{33}/\partial P$	$\partial C_{12}/\partial P$	$\partial C_{13}/\partial P$	$\partial C_{44}/\partial P$	$\partial C_{66}/\partial P$
This study	4.9(4)	5.6(5)	6.7(4)	1.5(3)	2.0(1)	2.3(2)

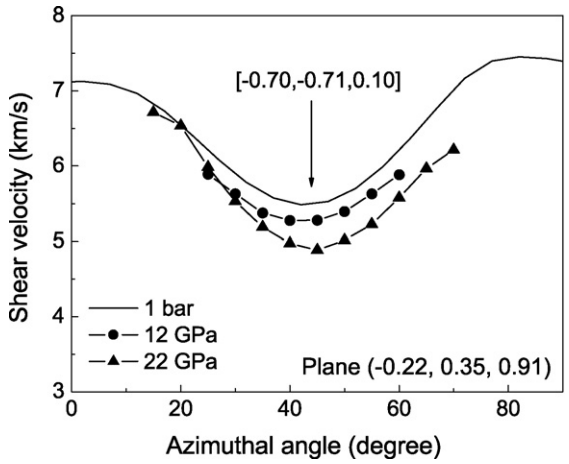

Fig. 4. Velocities of the slow shear wave in plane (−0.22, 0.35, 0.91) at various pressures showing softening of the shear wave with increase of pressure.

even larger than C'_{11} and C'_{33} (Table 1). By 12 GPa, C_{12} has increased about 40% compared to its ambient value, while C_{11} increased only 13% and C_{13} increased only about 10% over the examined pressure range. As a result, we observe a decrease of the combination $C_{11} - C_{12}$ with pressure (Fig. 3). The elastic constant $(C_{11} - C_{12})/2$ is associated with the transverse acoustic mode propagating along the [1 1 0] direction, and the decrease with pressure indicates mode softening consistent with theoretical predications (Cohen, 1992). Direct acoustic mode softening with increase of pressure in a direction close to [1 1 0] was observed in our experiment as shown in Fig. 4. The shear wave velocity along [−0.70, −0.71, 0.10] direction decreased about 11% upon compression to 22 GPa. It is expected that the acoustic mode softening should become enhanced when approaching the phase transition to the $CaCl_2$-type structure around 50 GPa (Kingma et al., 1995; Carpenter et al., 2000). This type of acoustic mode softening was reported in the isostructural SnO_2 system (Hellwig et al., 2003). Shieh et al. (2002) also reported experimental evidence of $(C_{11} - C_{12})/2$ softening in stishovite by inversion of measured lattice strains in radial X-ray diffraction experiments.

Fig. 5 shows the pressure dependences of the aggregate moduli: filled symbols are from the present study, lines are Eulerian finite strain fits. The bounds on aggregate moduli and their pressure derivatives are presented in Table 2 and compared with literature

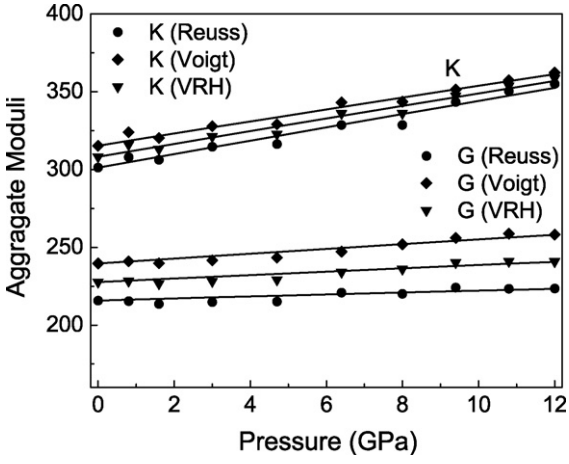

Fig. 5. Pressure dependences of the Voigt–Reuss–Hill average of aggregate moduli, as well as their Voigt and Reuss bounds.

Table 2
Aggregate elastic moduli and pressure derivatives at ambient temperature.

This study	Reuss	Voigt	VRH
K_{S0} (GPa)	301(1)	315(1)	308(1)
K_{T0} (GPa)	299(1)	313(1)	306(1)
G_0 (GPa)	216(1)	240(1)	228(1)
$(\partial K_S/\partial P)_{T0}$	4.34(16)	3.73(10)	4.0(1)
$(\partial K_T/\partial P)_{T0}$	4.4(2)	3.8(1)	4.0(1)
$(\partial G/\partial P)_0$	0.7(1)	1.5(1)	1.1(1)

VRH: Voigt–Reuss–Hill average.

values in Table 3. There exist large differences among the reported aggregate bulk modulus and pressure derivatives in static compression studies. These discrepancies arise in part because stishovite is highly incompressible and thus sensitive to non-hydrostatic stress. Another factor contributing to uncertainty in compression studies is the trade-off between K_{T0} and K'_{T0} in fitting pressure–volume data. In some studies, the K'_{T0} value was fixed (Ross et al., 1990; Liu et al., 1999; Andrault et al., 1998) (Table 3).

There are marked differences between the Reuss and Voigt bounds in the aggregate moduli (Fig. 5). The difference of bulk modulus for the two bounds decreased slightly from about 5% at ambient condition to 2% at 12 GPa, while the difference of shear modulus increased from 10.6% to 15.5%. These latter differences reflect the increase of elastic anisotropy, and are related to the lattice instability of the slow shear wave under compression.

By fitting our results to finite strain equations, we obtain the following pressure derivatives for the Reuss bounds on the aggregate moduli: $K'_{S0} = \partial K_{S0}/\partial P = 4.34(16)$ and $G'_0 = \partial G/\partial P = 0.7(1)$, and for the Voigt bounds: $K'_{S0} = \partial K_{S0}/\partial P = 3.73(10)$ and $G'_0 = \partial G/\partial P = 1.5(1)$, where the numbers in parentheses are $1-\sigma$ uncertainties in the last digit. These values are significantly lower than reported in an earlier polycrystalline ultrasonic study to 3 GPa ($K'_{S0} = 5.3(1)$; $G'_0 = 1.8(1)$; Li et al., 1996). Our results are in general agreement with theory (Karki et al., 1997): pressure dependences of C_{ij}s follow similar trends, and the differences in C_{ij}s at 1 bar are less than 6%. An isothermal compression curve for stishovite was constructed from our Brillouin experiment using the Reuss bound. Our compression curve (solid line) and its extrapolation to higher pressures (dashed lines) are in very good agreement with previous compression studies despite the differences in recovered parameters in those studies (Fig. 6).

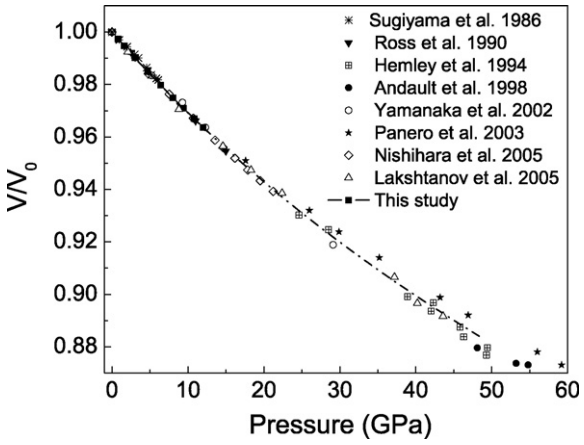

Fig. 6. Isothermal compression curve of stishovite calculated from the present study (solid line) and its extrapolation to higher pressures (dashed). Previous compression studies are shown for comparison. The samples of Lakshtanov et al. (2005) contained 1.8 wt.% Al_2O_3 and 500 ppm H_2O.

Table 3
Aggregate moduli and their pressure derivatives for stishovite.

Method	K_{T0}	K'_{T0}	G_0	G'_0	P_{max}	Medium	Reference
Brillouin	299(1)[a]	4.4(2)	216(1)	0.7(1)	12	MEW	This study
	306(2)[a]		208(2)		Ambient		Weidner et al. (1982)
	310(3)[a]		216(2)		Ambient		Brazhkin et al. (2005)
XRD	313(4)	6[b]			6	MEW	Sugiyama et al. (1987)
	313(4)	1.7(6)			16	ME	Ross et al. (1990)
	287(2)	6[b]					
	291(1)	4.3(1)			53	Annealing	Andrault et al. (1998)
	294(5)	5.3[b]			10	Boron epoxy	Liu et al. (1999)
	304[b]	4.6(1)			60		Shieh et al. (2002)
	292(13)	6[b]			29	MEW, Ar	Yamanaka et al. (2002)
	310(1)	4.6(2)			128	MEW/NaCl	Andrault et al. (2003)
	312.9(34)	4.8(2)			59	Annealing	Panero et al. (2003)
	297(5)	4.3(4)			22	NaCl	Nishihara et al. (2005)
Shock data	306(5)[c]	5.0(2)[c]			235		Luo et al. (2002)
Ultrasonic	305(5)[c]	5.3(1)[c]	217(4)	1.8(1)	3		Li et al. (1996)

K_{T0} and its pressure derivatives are Reuss bounds. ME: methanol–ethanol mixture (4:1) and MEW: methanol–ethanol–water mixture (16:3:1).
[a] Converted from adiabatic to isothermal.
[b] Fixed value.
[c] Adiabatic values.

Fig. 7 shows calculated aggregate sound velocities of stishovite at pressures up to 12 GPa at 300 K in comparison with a theoretical calculation at 0 K (Karki et al., 1997) and a low-pressure ultrasonic experimental study (Li et al., 1996). Aggregate sound velocities from a Brillouin spectroscopic study at room pressure are also shown (Weidner et al., 1982). Our results are in good agreement with the other two studies except those by Li et al. (1996) in which case polycrystalline samples were used. The velocities were expected to be lower for polycrystalline samples because of porosity especially at lower pressures (Li et al., 1996).

The azimuthal anisotropies are defined as $(V_{S,Max} - V_{S,Min})/V_{S,aggr}$ for S-waves (regardless of polarization) and $(V_{P,Max} - V_{P,Min})/V_{P,aggr}$ for P-waves, respectively. The calculated P-wave anisotropy decreased from 24 to 22%, while S-wave anisotropy increased from 43 to 49% upon compression to 12 GPa. The increase of S-wave anisotropy with compression reflects the increased structural anisotropy as the phase transformation is approached (Karki et al., 1997).

For tetragonal crystals, the linear compressibility, β, is defined by (Nye, 1985):

$$\beta = (S_{11} + S_{12} + S_{13}) - (S_{11} + S_{12} - S_{13} - S_{33})n_3^2$$

where n_3 is the direction cosine with the c-axis, and S_{ij} are the elastic compliances. Fig. 8 shows the linear compressibility curves at various pressures. The a-axis is more compressible than the c-axis. The a-axis compressibility, β_a, decreased from 1.3×10^{-3} GPa^{-1} to 1.1×10^{-3} GPa^{-1} upon compression to 12 GPa. It is interesting to note that linear compressibility β_c increased slightly from 0.64×10^{-3} GPa^{-1} at ambient condition to 0.65×10^{-3} GPa^{-1} at 12 GPa. Our linear compressibilities are generally consistent with results from X-ray data (Sugiyama et al., 1987; Ross et al., 1990).

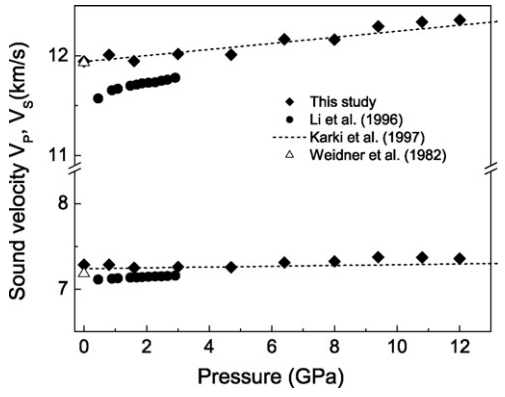

Fig. 7. Aggregate sound velocities of stishovite at 300 K in comparison with previous studies: Weidner et al. (1982), Li et al. (1996), and Karki et al. (1997).

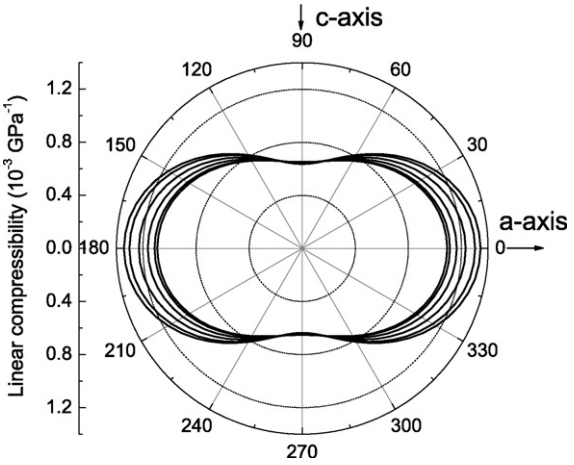

Fig. 8. Anisotropy of linear compressibility at various pressures in a–c plane: 1 bar, 1.6, 4.7, 8.0, 11.0, and 12.0 GPa, respectively, from outer to inner curves.

In summary, we have reported the first measurements of the full set of elastic constants of stishovite to 12 GPa, and report selected acoustic velocities to 22 GPa. The pressure derivative of the bulk and shear moduli are lower than reported in previous ultrasonic studies. Further studies are warranted to constrain the elasticity at higher pressure conditions.

Acknowledgements

We thank Yingwei Fei of the Geophysical Laboratory, Carnegie Institution of Washington, for access to his high-pressure multi-anvil apparatus for sample synthesis. V.V. Brazhkin also provided additional stishovite single crystalline samples, fabricated by the N.A. Bendeliani group, that were used to confirm results in specific directions at 1 bar. J. Hu is acknowledged for her assistance with X-

ray diffraction measurement at X17C, National Synchrotron Light Source, Brookhaven National Laboratory. This work was support by NSF and C-DAC (Carnegie DOE Alliance Center). Use of X17C at NSLS is supported by DOE (US-DOE contract DE-AC02-10866) and COMPRES (NSF Cooperative Agreement EAR 06-49658).

References

Akaogi, M., Yusa, H., Shiraishi, K., Suzuki, T., 1995. Thermodynamic properties of α-quartz, coesite, and stishovite and equilibrium phase relations at high pressures and high temperatures. J. Geophys. Res. 100, 22337–22347.

Andrault, D., Fiquet, G., Guyot, F., Hanfland, M., 1998. Pressure induced landau-type transition in stishovite. Science 282, 720–724.

Andrault, D., Angel, R.J., Mosenfelder, J.L., Le Bihan, T., 2003. Equation of state of stishovite to lower mantle pressures. Am. Miner. 88, 301–307.

Bendeliani, N.A., 2002. Hydrothermal growth of stishovite (SiO_2). Physics-Uspekhi 45, 444–445.

Birch, F., 1978. Finite strain isotherm and velocities for single-crystal and polycrystalline NaCl at high pressures and 300 K. J. Geophys. Res. 83, 1257–1264.

Brazhkin, V.V., Grimsditch, M., Guedes, I., Bendeliani, N.A., Dyuzheva, T.I., Lityagina, L.M., 2002. Elastic moduli and the mechanical properties of stishovite single crystals. Physics-Uspekhi 45, 447–448.

Brazhkin, V.V., McNeil, L.E., Grimsditch, M., Bendeliani, N.A., Dyuzheva, T.I., Lityagina, L.M., 2005. Elastic constants of stishovite up to its amorphization temperature. J. Phys.: Condens. Matter 17, 1869–1875.

Bromiley, G.D., Bromiley, F.A., David, W.B., 2006. On the mechanisms for H and Al incorporation in stishovite. Phys. Chem. Miner. 33, 613–621.

Carpenter, M.A., Hemley, R.J., Mao, H.-K., 2000. High-pressure elasticity of stishovite and the $P4(2)/mnm \leftrightarrow Pnnm$ phase transition. J. Geophys. Res. 105, 10807–10816.

Cohen, R.E., 1992. First-principles predictions of elasticity and phase transitions in high pressure SiO_2 and geophysical implications. In: Syono, Y., Manghnani, M.H. (Eds.), High Pressure Research: Application to Earth and Planetary Sciences. AGU, Washington, DC, p. 425.

Dobrzhinetskaya, L.F., Green, H.W., 2007. Experimental studies of mineralogical assemblages of metasedimentary rocks at Earth's mantle transition zone conditions. J. Met. Geol. 25, 83–96.

Gwanmesia, G.D., Liebermann, R.C., 1992. Polycrystals of high-pressure phases of mantle minerals: hot pressing and characterization of physical properties. In: Syono, Y., Manghnani, M.H. (Eds.), High Pressure Research: Application to Earth and Planetary Sciences. AGU, Washington, DC, pp. 117–135.

Hemley, R.J., Mao, H.-K., Chao, E.C.T., 1986. Raman spectrum of natural and synthetic stishovite. Phys. Chem. Miner. 13, 285–290.

Hemley, R.J., Prewitt, C.T., Kingma, K.J., 1994. High-pressure behavior of silica. In silica: physical behavior, geochemistry and materials applications. Rev. Miner. Geochem. 29, 41–81.

Hemley, R.J., Shu, J., Carpenter, M.A., Hu, J., Mao, H.-K., Kingma, K.J., 2000. Strain/order parameter coupling in the ferroelastic transition in dense SiO_2. Solid State Commun. 114, 527–532.

Hirose, K., Fei, Y.W., 2002. Subsolidus and melting phase relations of basaltic composition in the uppermost lower mantle. Geochim. Cosmochim. Acta 66, 2099–2108.

Hellwig, H., Goncharov, A.F., Gregoryanz, E., Mao, H.-K., Hemley, R.J., 2003. Brillouin and Raman spectroscopy of the ferroelastic rutile-to-$CaCl_2$ transition in SnO_2 at high pressure. Phys. Rev. B 67, 174110.

Holm, B., Ahuja, R., 1999. *Ab initio* calculation of elastic constants of SiO_2 stishovite and α-quartz. Phys. Rev. B 111, 2071–2074.

Irifune, T., Ringwood, A.E., 1993. Phase transformations in subducted oceanic crust and buoyancy relationships at depths of 600–800 km in the mantle. Earth Planet. Sci. Lett. 117, 101–110.

Irifune, T., Ringwood, A.E., Hibberson, W.O., 1994. Subduction of continental crust and terrigenous and pelagic sediments: an experimental study. Earth Planet. Sci. Lett. 126, 351–368.

Jiang, F., Speziale, S., Duffy, T.S., 2004. Single-crystal elasticity of grossular- and almandine-rich garnets to 11 GPa by Brillouin scattering. J. Geophys. Res. 109, B10210.

Karki, B.B., Stixrude, L., Crain, J., 1997. *Ab initio* elasticity of three high-pressure polymorphs of silica. Geophys. Res. Lett. 24, 3269–3272.

Karki, B.B., Stixrude, L., Wentzcovitch, R.M., 2001. High-pressure elastic properties of major materials of Earth's mantle from first principles. Rev. Geophys. 39, 507–534.

Kesson, S.E., Fitz Gerald, J.D., Shelley, J.M.G., 1994. Mineral chemistry and density of subducted basaltic crust at lower-mantle pressures. Nature 372, 767–769.

Kingma, K.J., Cohen, R.E., Hemley, R.J., Mao, H.-K., 1995. Transformation of stishovite to a denser phase at lower-mantle pressures. Nature 374, 243–245.

Lakshtanov, D.L., Vanpeteghem, C.B., Jackson, J.M., Bass, J.D., Shen, G., Prakapenka, V.B., Litasov, K., Ohtani, E., 2005. The equation of state of Al, H-bearing SiO_2 stishovite to 58 GPa. Phys. Chem. Miner. 32, 466–470.

Lakshtanov, D.L., Litasov, K.D., Sinogeikin, S.V., Hellwig, H., Li, J., Ohtani, E., Bass, J.D., 2007a. Effect of Al^{3+} and H^+ on the elastic properties of stishovite. Am. Miner. 92, 1026–1030.

Lakshtanov, D.L., Sinogeikin, S.V., Litasov, K.D., Prakapenka, V.B., Hellwig, H., Wang, J., Sanches-Valle, C., Perrilat, J., Chen, B., Somayazulu, M., Li, J., Ohtani, E., Bass, J.D., 2007b. The post-stishovite phase transition in hydrous alumina-bearing SiO_2 in the lower mantle of the earth. Proc. Natl. Acad. Sci. U.S.A. 104, 13588–13590.

Li, B.S., Rigden, S.M., Liebermann, R.C., 1996. Elasticity of stishovite at high pressure. Phys. Earth Planet. Inter. 96, 113–127.

Liu, J., Zhang, J., Flesch, L., Li, B., Weidner, D.J., Liebermann, R.C., 1999. Thermal equation of state of stishovite. Phys. Earth Planet. Inter. 112, 257–266.

Litasov, K.D., Hiroyuki, K., Shatskiy, A., Ohtani, E., Lakshtanov, D.L., Bass, J.D., Ito, E., 2007. High hydrogen solubility in Al-rich stishovite and water transport in the lower mantle. Earth Planet. Sci. Lett. 262, 620–634.

Luo, S.N., Mosenfelder, J.L., Asimow, P.D., Ahrens, T.J., 2002. Direct shock wave loading of stishovite to 235 GPa: implications for perovskite stability relative to an oxide assemblage at lower mantle conditions. Geophys. Res. Lett. 29, 361–364.

Nishihara, Y., Nakayama, K., Takahashi, E., Iguchi, T., Funakoshi, K., 2005. *P–V–T* equation of state of stishovite to the mantle transition zone conditions. Phys. Chem. Miner. 31, 660–670.

Nye, J.F., 1985. Physical Properties of Crystals: Their Representation by Tensors and Matrices. Clarendon Press, Oxford, p. 329.

Ono, S., Takuma, S., Hirose, K., Kuwayama, Y., Komabayashi, T., Kikegawa, T., 2002. Equation of state of Al-bearing stishovite to 40 GPa and 300 K. Am. Miner. 87, 1486–1489.

Panero, W.R., Benedetti, L.R., Jeanloz, R., 2003. Equation of state of stishovite and interpretation of SiO_2 shock-compression data. J. Geophys. Res. 108, 2015.

Panero, W.R., Stixrude, L., 2004. Hydrogen incorporation in stishovite at high pressure and symmetric hydrogen bonding in δ-AlOOH. Earth Planet. Sci. Lett. 221, 421–431.

Pawley, A.R., McMillan, P.F., Holloway, J.R., 1993. Hydrogen in stishovite, with implications for mantle water content. Science 261, 1024–1026.

Ross, N.L., Shu, J., Hazen, R.M., Gasparik, T., 1990. High-pressure crystal chemistry of stishovite. Am. Miner. 75, 739–747.

Shieh, S.R., Duffy, T.S., Li, B., 2002. Strength and elasticity of SiO_2 across the stishovite–$CaCl_2$-type structural phase boundary. Phys. Rev. Lett. 89, 255507.

Speziale, S., Duffy, T.S., 2002. Single-crystal elastic constants of fluorite (CaF_2) to 9.3 GPa. Phys. Chem. Miner. 29, 465–472.

Speziale, S., Duffy, T.S., Angel, R.J., 2004. Single-crystal elasticity of fayalite to 12 GPa. J. Geophys. Res. 109, B12202.

Sugiyama, M., Endo, S., Koto, K., 1987. The crystal structure of stishovite under pressure up to 6 GPa. Miner. J. 13, 455–466.

Vinnik, L., Kato, M., Kawakatsu, H., 2001. Search for seismic discontinuities in the lower mantle. Geophys. J. Int. 147, 41–56.

Weidner, D.J., Bass, J.D., Ringwood, A.E., Sinclair, W., 1982. The single-crystal elastic-moduli of stishovite. J. Geophys. Res. 87, 4740–4746.

Yamanaka, T., Fukuda, T., Tsuchiya, J., 2002. Bonding character of SiO_2 stishovite under high pressures up to 30 GPa. Phys. Chem. Miner. 29, 633–641.